Review Article

Metal/Metal-Oxide Nanoclusters for Gas Sensor Applications

Ahmad I. Ayesh

Department of Mathematics, Statistics and Physics, Qatar University, Doha, Qatar

Correspondence should be addressed to Ahmad I. Ayesh; ayesh@qu.edu.qa

The development of gas sensors that are based on metal/metal-oxide nanoclusters has attracted intensive research interest in the last years. Nanoclusters are suitable candidates for gas sensor applications because of their large surface-to-volume ratio that can be utilized for selective and rapid detection of various gaseous species with low-power consuming electronics. Herein, nanoclusters are used as building blocks for the construction of gas sensor where the electrical conductivity of the nanoclusters changes dramatically upon exposure to the target gas. In this review, recent progress in the fabrication of size-selected metallic nanoclusters and their utilization for gas sensor applications is presented. Special focus will be given to the enhancement of the sensing performance through the rational functionalization and utilization of different nanocluster materials.

1. Introduction

A sensor is a device that produces a response upon exposure to some stimulus through introducing functionally related output. The response is an alert in one or more of the sensor properties such as mass, electrical conductivity, and capacitance. Therefore, sensors enable us to monitor the environment around us and to use that information for different purposes [1]. Nanotechnology is enabling the production of efficient sensors with broad range of applications. The unique properties of the nanomaterials make them suitable candidates for sensitive detection of chemical and biological species [2] because they exhibit great adsorptive capacity due to the large surface-to-volume ratio, produce great modulation of the electrical signal upon exposer to analytes due to the great interaction zone over the cross sectional area (Debye length), enable tuning electrical properties by controlling the composition and the size of the nanomaterial, and ease configuration and integration in low-power microelectronic systems.

In this review we will focus on the conductometric (or resistive) transducers. Therefore, the review will introduce the operation principle of the nanostructure conductometric gas sensors and the fabrication of nanocluster devices. Next, recent progress in conductometric nanocluster gas sensors will be presented. Lastly, the review will be summarized with possible future developments in gas sensors.

2. Nanostructure Conductometric Gas Sensors

Nanomaterials are classified depending on their dimensions into three categories: zero-, one-, and two-dimensional nanomaterials. In order to use those materials for gas sensing applications, they should have suitable composition and morphologies [3]. This review focuses on nanomaterials of zero-dimensions (or nanoclusters). Nanoclusters are defined as aggregates of atoms (or small nanoparticles) that are in nanometer size and their properties are different from their bulk equivalents. The synthetic conditions to obtain nanoclusters are so broad, ranging from chemical methods at different temperatures and/or pressures to physical methods where nanoclusters could be formed from the atomic vapor.

A conductometric transduce consists of (i) layer of gas sensitive material, (ii) substrate, (iii) electrodes to measure the electrical signals, and (iv) heater. The basic structure of a typical conductometric transducer is shown schematically in Figure 1. The contacts could be of Ohmic or Schottky type, and their geometry controls the sensor operational mode. The conductance (or the resistance) of the sensor is dependent on the properties of the sensitive material, concentration of the target gas, and the measurement parameters such as the temperature and applied voltage. The reaction of the target gas with the sensitive material takes place at different sites of the structure depending on the morphology and is transduced into electrical signal.
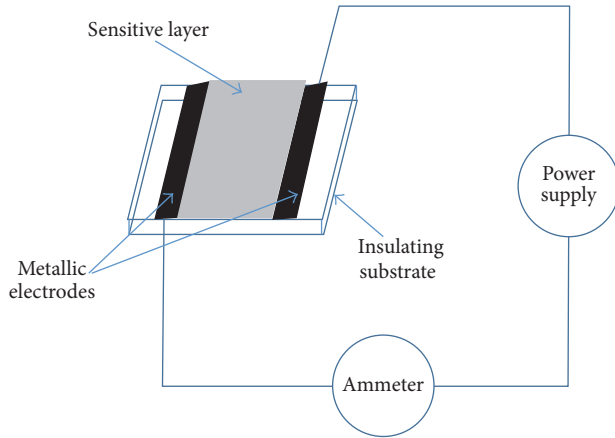
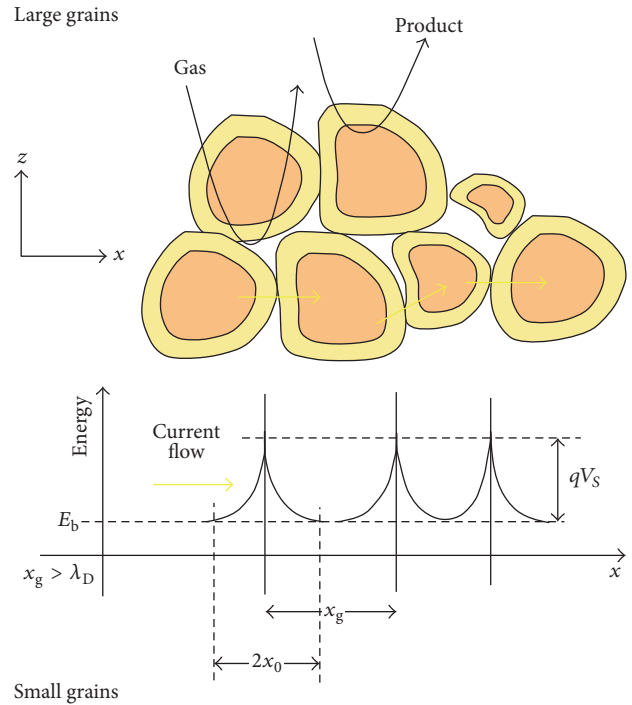FIGURE 1: Schematic representation of the conductometric transducer.

FIGURE 2: Schematic representation of a porous sensing layer with geometry and energy band. λ_D is the Debye length, x_g is the grain size, and x_0 is the depth of the depletion layer. © IOP Publishing. Reproduced with permission. All rights reserved [11].

The gas sensitive material could be made of bulk or grains that have sizes in the micro- or nanorange. The sensitive material could be completely or partially depleted depending on its thickness, porosity, and the Debye length λ_D. Various sensitive materials are prepared and deposited as thick film, thin film, or incorporated into transducers for gas sensing applications [4–9]. The sensor performance depends on the porosity and the sensitivity of the material. In addition, charge transport depends on the percolation path through intergranular regions. Therefore, by changing small details in the preparation process, each sensor differs in its sensing characteristics.

The sensitive layer could be compact of porous material; see Figure 2 [10]. When the sensitive layer consists mainly of compact material with a thickness larger than the Debye length, it can only partially be depleted when exposed to a gas; thus, the interaction does not affect the entire sensitive layer. Accordingly, two levels of the resistance into parallel are introduced with only the underneath layer of the sensitive layer being in contact with the electrodes. Therefore, thin porous sensitive layer should function better for the gas sensing application.

A main advantage of the gas sensors made of porous nanostructured thin films is that the volume of the nanostructure is accessible to the gases where the active surface is much higher than the geometric one, unlike the sensors made of compact layers where the interaction takes place only at the surface layer of the sensor (this is the case for most of the thick film based sensors). For gas sensors with nanostructured porous structure, where necks might be present between the grains, it is possible to have interaction between the target gas with surface/bulk for large necks, grain boundaries for large grains, and flat bands for small grains and small necks. For small grains and narrow necks a surface influence on charge carrier mobility should be taken into consideration when the mean free path of free charge carriers becomes comparable with the dimension of the grains. The number of collisions experienced by the free charge carriers in the bulk of the grain becomes comparable with the number of surface collisions.

Consequently, the number of collisions may be influenced by adsorbed species acting as additional scattering centres.

Contacts in gas sensors made of thin film of nanoclusters have dominating effect on the resistance. Direct current measurements and AC impedance spectroscopy could be used to identify the contact related elements. They also can be used to identify the presence of surface regions since the depletion region behaves like a capacitor [8]. Each type of contribution in a sensing layer can be simulated to an equivalent circuit. Those equivalent circuits can be extrapolated from detailed critical analysis of the experimental electrical measurements, morphology of the sensing layer, and microscopic characteristics of the sensing layer and sensor. For Schottky contact type, a simple approximation can be performed based on the fact that the total charge trapped on the surface level, Q_S, can be written as [18]

$$Q_S = qn_b s z_0, \tag{1}$$

where q is the electron charge, n_b is the electron concentration, s is the total surface where the adsorption take place, and z_0 is the depth of the depletion region. The relation between the surface charge and band bending (V_S) is [10]

$$Q_S = s\sqrt{2q\varepsilon\varepsilon_0 n_b V_S}, \tag{2}$$

where ε_0 and ε are the air permittivity and the media relative permittivity. It should be noted that, in this approximation, it is assumed that all the electrons in the conduction band from

the depletion layer are captured on the surface trap levels. The capacitance of the depletion region can be given as

$$C_s = \frac{1}{s}\left(\frac{\partial Q_S}{\partial V_S}\right) = \sqrt{\frac{q\varepsilon\varepsilon_0 n_b}{2V_S}} \qquad (3)$$

AC impedance spectroscopy is a useful characterization technique that can be used to identify the sensor equivalent circuit and the determination of the values of circuit elements, that is, resistances and capacitances. Once equivalent circuits are accompanied with the above equations, one can optimize the sensors' parameters via modifying layer fabrication technology [19–22] and isolate the influence of the target gas (for example, O_2, H_2O, CO, CH_4, O_3, and NO) on the different components of the sensor [11, 23–26].

Following the above discussion, the sensing performance of a transducer is greatly affected by the choice of the sensitive layer thickness on different transducer platforms [27–32], as well as the electrode position/spacing [28, 33, 34]. The effect of the former was investigated at different ambient conditions [18]. In the latter [11], sensing layers with interdigitated electrodes having different spacing in the range 10–50 μm for SnO_2 films were used [11]. The results show that the resistance increases with the electrode spacing and decreases with the thickness of the sensitive layer for air and NO_2, although the results show that the resistance is independent of layer thickness or electrode spacing for the CO case.

Typically, gas sensors are operated in ambient air where they are exposed to humidity and interfering gases such as oxygen and carbon dioxide. Those gases may form bonds with the surface of the nanoclusters by exchanging electrons; thus, they may form dipoles. Since dipoles do not affect the concentration of the free charge carriers, they do not have an effect on the resistance of sensor sensitive layer. As an example, Figure 3 shows the case of oxygen and hydroxyl groups (as dipoles) where they are bounded to the surface of an n-type semiconductor [11]. Their effects are mainly the band bending and change of the electronic affinity of the semiconductor when compared to the situation existing before the adsorption.

In the temperature range between 100 and 500°C, oxygen may ionosorb over the surface of the nanoclusters either in the molecular (O_2^-) or in atomic (O^-) forms. At high temperatures, O^- is dominant while at temperatures of 200°C or below O_2^- is more dominant since it has lower activation energy. The interaction with oxygen creates a depletion layer at the nanocluster surface; thus, a barrier potential has to be overcome by electrons to reach the nanocluster surface [10]. The chemisorption of oxygen can be described as [10]

$$\frac{\beta}{2}O_2^{gas} + \alpha e^- + S \longleftrightarrow O_{\beta S}^{-\alpha}, \qquad (4)$$
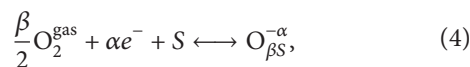
where O_2^{gas} is oxygen in the molecular form in ambient atmosphere, e^- is the electron that has sufficient energy to reach to the nanocluster surface, S is an unoccupied chemisorption site for oxygen, $O_{\beta S}^{-\alpha}$ is the chemisorbed oxygen species, and $\alpha = 1$ or 2 for singly or doubly ionized forms, respectively. $\beta = 1$ or 2 for atomic or molecular forms, respectively.
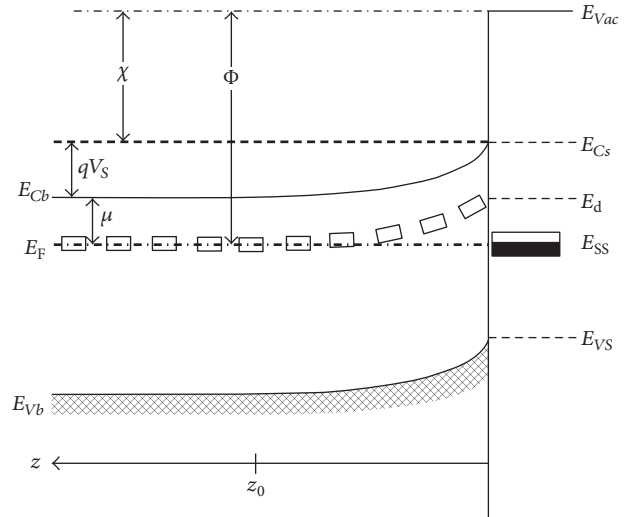

Figure 3: Band bending after chemisorption of charged species (e.g., ionosorption of oxygen on E_{SS} levels). Φ denotes the work function, χ is the electron affinity, and μ is the electrochemical potential. © IOP Publishing. Reproduced with permission. All rights reserved [11].

For some reducing gases, gas detection is related to the reactions between the species to be detected and ionosorbed surface oxygen. When a reducing gas like CO comes into contact with the surface, the following reactions may take place:

$$CO_{gas} \longrightarrow CO_{ads} \qquad (5)$$

$$CO_{ads} + O_{ads}^{\;-} \longrightarrow CO_{2,gas} + e^- \qquad (6)$$
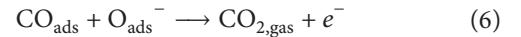
These consume ionosorbed oxygen which change the density of ionosorbed oxygen that is detected and in turn change the electrical conductance of metal nanocluster.

Direct adsorption is also possible for gases such as NO_2 which is strongly electronegative.

$$NO_{2,gas} \longleftrightarrow NO_{2,ads} \qquad (7)$$

$$e^- + NO_{2,ads} \longleftrightarrow NO_{2,ads}^{\;-} \qquad (8)$$
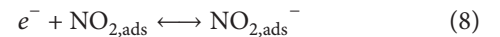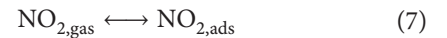
Therefore, the occupation of surface states, which are much deeper in the band gap than oxygen, increases the surface potential and reduces the overall sensor conductance. Using the Schottky approximations for nanoclusters with diameter (D) less than or equal to Debye length ($D \leq \lambda_D$), the energy barrier ΔE can be written as [35]

$$\Delta E \sim k_B T \left(\frac{R}{2\lambda_D}\right) \qquad (9)$$

with $\lambda_D = \sqrt{\varepsilon\varepsilon_0 k_B T / q^2 n_b}$. Here, k_B is the Boltzmann constant, T is the temperature in Kelvin, and R is the radius of the nanocluster. Therefore, if ΔE is comparable with the thermal energy, a homogeneous electron concentration in the grain will result, which in turn produces flat band energy.
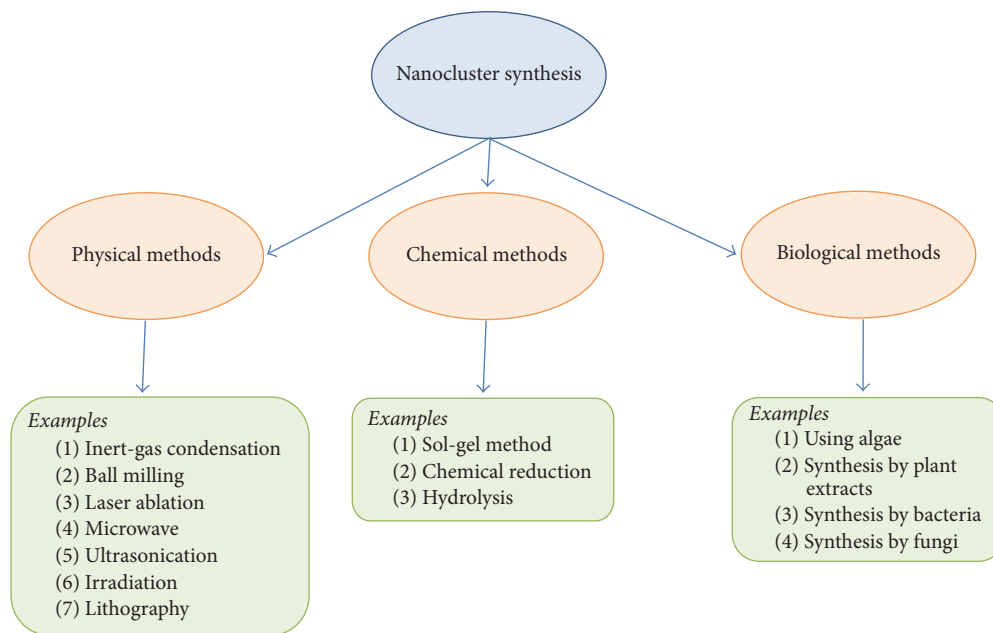
Nanocluster synthesis

Physical methods

Chemical methods

Biological methods

Examples
(1) Inert-gas condensation
(2) Ball milling
(3) Laser ablation
(4) Microwave
(5) Ultrasonication
(6) Irradiation
(7) Lithography

Examples
(1) Sol-gel method
(2) Chemical reduction
(3) Hydrolysis

Examples
(1) Using algae
(2) Synthesis by plant
     extracts
(3) Synthesis by bacteria
(4) Synthesis by fungi

FIGURE 4: Illustration of the different nanocluster synthesis methods.

3. Nanocluster Device Fabrication

Because of the wide availability of synthesis and processing of nanomaterials, a careful selection of methodology to prepare nanoclusters of sufficiently fine dispersion, porous structure, high crystallinity, and bulk quantity is required. Nevertheless, new material science and physics await discovery and remain to be explored based on the newly acquired nanoscience and nanotechnology knowledge.

Nanoclusters can be synthesized using different chemical and physical methods with many examples that can be found in the literatures [36–41]. Those synthesis methods include (a) physical synthesis such as inert gas condensation, ball milling, laser ablation, and others; (b) chemical synthesis such as sol-gel, chemical reduction, hydrolysis, and others; and (c) biological synthesis that can be established using algae, plant extracts, bacteria, fungi, yeast, and others. A summary of those methods is presented in Figure 4. Although examples of the usage of nanoclusters synthesized using different methods for gas sensing applications will be presented in this review, special focus will be given to nanocluster synthesis using the inert gas condensation technique because of its many advantages as discussed below [42–45].

Sputtering and inert gas condensation inside an ultra-high vacuum chamber is a unique technique for producing high quality nanoclusters of many advantages including the following [46, 47]: (i) the nanoclusters are of high purity as they are prepared by inert gas inside ultra-high vacuum [48]; (ii) the size of the nanoclusters that can be tuned *easily* within a range of sizes corresponding to the source design by controlling the source conditions (as discussed below) [49]; (iii) the produced nanoclusters being charged which allow the size selection of the nanoclusters using a suitable mass filter [48]; (iv) the narrow size distribution of the

produced nanoclusters [13]; (v) the produced nanoclusters which may self-assemble directly on device substrate without the need of any additional experimental steps [50]; (vi) the coverage of the deposited nanoclusters on the substrate (and, thus, the sensitive layer thickness is quit controlled by controlling the deposition time) [51]; (vii) the composition of the produced nanoclusters which is controlled by controlling the composition of the target material [52]; and (viii) the technique that could be used on a commercial scale.

A typical example of an ultra-high vacuum system that can be used for nanocluster fabrication is shown in Figure 5 [12]. The system consists of the following main parts: (i) source chamber where nanoclusters are produced, (ii) deposition chamber where the nanoclusters are deposited on the substrate, and (iii) quadrupole mass filter (QMF) that is used for investigating the nanocluster size distribution or selecting nanoclusters of a particular size.

3.1. Nanocluster Production. To produce nanoclusters of a particular metal, a target of the metal is fixed on the sputter head [53]. The system is then pumped down to a desirable pressure prior the nanocluster production. A high negative DC voltage is applied to the target, and an inert gas (typically argon) is injected inside the source chamber. Consequently, plasma is ignited [54]. Herein, the inert gas plays three major roles: (i) producing the plasma required to sputter the metal from the target, (ii) establishing inert gas condensation of the sputtered material, and (iii) creating pressure gradient between the source chamber and the deposition chamber which introduce the nanoclusters to the deposition chamber through the QMF.

The main factors that determine the nanocluster size are the distance from the target surface to the exit nozzle of the source (defined as the aggregation length (L)), inert
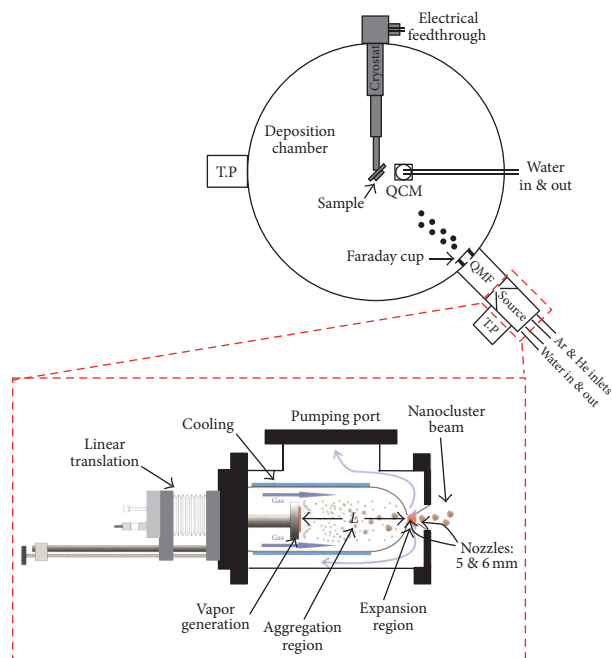
FIGURE 5: Schematic diagram of the ultra-high vacuum compatible nanocluster system and the nanocluster source. Reprinted with Springer permission from [12].

gas flow rate (f), and sputtering discharge power (P). The sputter head is mounted on a linear translator with a motor, where its position and, thus, L can be varied without venting the source chamber. An example of the investigation of these factors for Pd nanoclusters is shown in Figure 6 [49]. Here, the three factors (L, f, and P) could be tuned to generate nanoclusters of the required average size. In general, increasing the aggregation length increases the time spent by the nanoclusters inside the source chamber (growth region); thus, their sizes increase. However, the relation between the nanocluster size and both f and P is not a simple relation and it depends on the nanocluster formation mechanism(s). Hence, it is subject of investigation by different research groups [55–57]. Herein, the above three factors have to be fine-tuned for each type of nanoclusters to achieve the required nanocluster size.

The QMF consists of four parallel metal rods where each pair of opposite rods is connected together electrically to potentials of ($U + V\cos(\omega t)$) and $-(U + V\cos(\omega t))$; here U is a DC voltage and $V\cos(\omega t)$ is an AC voltage [58]. In each size distribution scan, the ratio U/V is fixed and the mass distribution is scanned by varying the frequency, ω. The resolution of the filter is adjusted for a mass scan by setting the U/V ratio. The U/V ratio is activated as a function of the mass number such that the actual resolution $\Delta M/M$ does not remain constant but ΔM does [59]. A grid located at the exit of the mass filter (Faraday cup) can be used to measure the ion flux of the selected mass/size, and the resultant current is measured by a picoammeter. Therefore, the current signal reflects the population/number of the produced nanoclusters.

3.2. Substrate Preparation.

The most common gas sensor structures presented in the literature are the two-point and field-effect transistor (FET) structures (see Figure 7). Sensors based on both structures rely on changes of electrical resistivity/conductivity of the gas sensitive layer (nanocluster film) due to the interaction with the surrounding atmosphere.

Gas sensors based on the two-point structure are made of two metallic electrodes with proper spacing and a film of nanoclusters. Herein, planar metallic electrodes of interdigitated structure are appropriate to be used for the electrical contact of materials [60]. The dimensions of the spacing between the electrodes need to be optimized for each type of sensor, as discussed below.

A typical structure of the FET sensor consists of a conducting substrate coated with an insulating layer that represents the gate (e.g., SiO_2/doped-Si). Two metallic electrodes are deposited on an insulating substrate and they serve as source and drain. The active nanocluster layer is deposited between the source and drain electrodes, and it acts as the channel of the FET. The resistance of the active layer can be changed by the field-effect created by applying a potential to the gate: here, the gate is the doped-Si substrate. The charge transfer process induced by surface reactions determines the sensor resistance. The current flows parallel to the surface and is modulated by the gate voltage for the channel of a FET or by increasing the sensor temperature for the two-point structure. When the channel is fully depleted, carriers thermally activated from surface states are responsible for conduction.

The metal electrodes can be made by photolithography and microfabrication technology on an insulator substrate such as glass (for the two-point structure) and SiO_2/doped-Si (for FET and two-point structures). Figure 7 shows schematic diagram of an interdigitated electrode structure and the steps included in the photolithography process. Photolithography is the process of transferring geometric shapes on a mask to the surface of a substrate. The steps involved in the photolithographic process are substrate cleaning; insulator layer formation (for the case of doped-Si wafers); photoresist application; exposure to UV light through a mask and development; metal contact evaporation; and lift-off all of the photoresist. In the first step, the substrates/wafers are chemically cleaned to remove particulate matter on the surface as well as any traces of organic, ionic, and metallic impurities. If Si wafers are used, silicon dioxide (or silicon nitride), which serves as an insulating layer, is grown on the surface of the wafer. After the formation of the insulating layer, positive photoresist is applied to the surface of the wafer using spin coating which produces a thin uniform layer of photoresist on the substrate/wafer surface. The photoresist is exposed to UV light through a *mask* (a glass plate with a patterned emulsion of metal film on one side); here, the exposed photoresist will be removed. Exposure to the UV light changes the chemical structure of the photoresist so that it becomes more soluble in the developer. The exposed resist is then washed away by a developer solution, leaving windows of the bare underlying substrate. The mask, therefore, contains an exact copy of the metallic contact pattern which is to remain on the wafer. Next step includes metallic contact fabrication by a thin
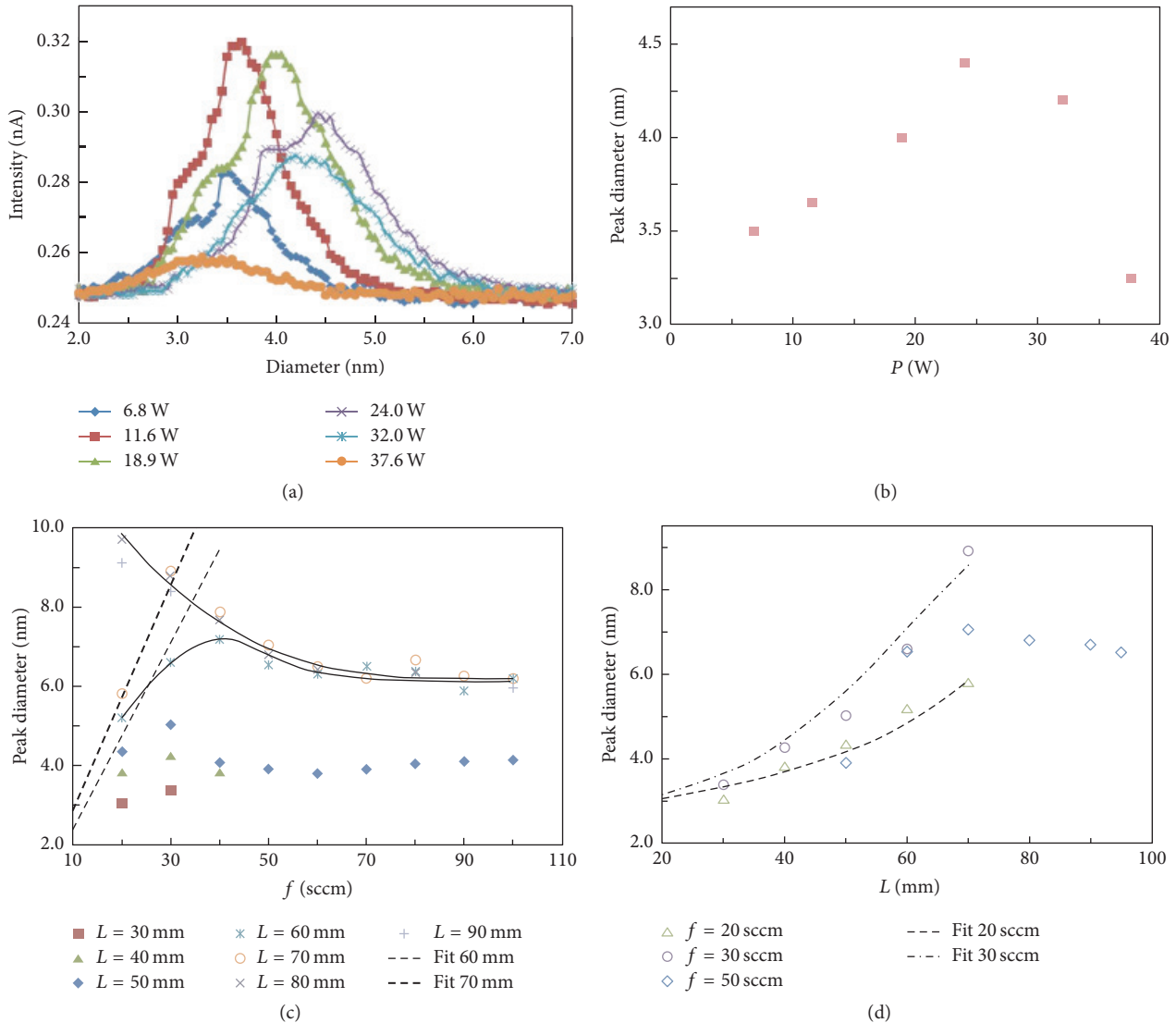
FIGURE 6: (a) The effect of the sputtering discharge power on the nanocluster size distribution. (b) The dependence of the peak diameter on the sputtering discharge power. (c) The dependence of the peak diameter on Ar flow rate for aggregations lengths in the range of 30–90 mm. The dashed lines are the theoretical nanocluster size calculation for $L = 60$ and 70 mm. The solid lines serve as guide to the eye to show zone I increase in the peak diameter with f for $L = 60$ mm and $f = 40$ sccm and zone II decrease in the peak diameter with f for $L = 80$ mm or for $L = 60$ mm and $f = 40$ sccm. (d) The dependence of the peak diameter on L for $f = 20$, 30, and 50 sccm. The dashed lines are the theoretical nanocluster size calculations for $f = 20$ and 30 sccm. Reprinted with AIP permission from [13].

film evaporator that utilizes either thermal evaporation or sputtering. Finally, the substrate is placed inside hot acetone to left-off all of the photoresist keeping the substrate with the metallic electrodes according to the pattern on the used mask.

3.3. Device Fabrication. A directed beam of nanoclusters exits from the QMF and is deposited on the substrate (see Figure 6). The produced nanoclusters are deposited on the sensor substrate that is fixed on a cryostat finger or on a sample holder which is mounted on a vertical motorized linear translator. The nanocluster deposition rate is measured using a quartz crystal monitor (QCM). The QCM is fixed on a motorized linear translator that enables driving the QCM

in front of the exit nozzle, check the deposition rate, and then drive it back away from the beam path.

The produced nanoclusters are deposited on an insulating substrate with preformed Au/NiCr contacts. The electrical conductivity of the sample is observed during nanocluster deposition; see Figure 8. A sharp rise in the conductivity indicates completion of at least one continuous network of nanoclusters between the contacts. Consequently, the nanocluster deposition can be suddenly stopped using an automatic shutter at the onset of conduction (percolation threshold) or keep the deposition for longer time to create a thicker film of nanoclusters. Electrical measurements can be performed subsequently on the sample as a function of the target gas type and concentration at controlled temperature.

Metal electrode

Metal electrode

(a)

| Metal electrode |
| Insulating substrate |

(b)

| Metal electrode |
| Insulating substrate |
| Doped-Si: back gate |

(c)

UV radiation

Mask

Photoresist

SiO_2

Doped-Si

Exposed photoresist

SiO_2

Doped-Si

Developed photoresist

SiO_2

Doped-Si

Metal deposition

Au

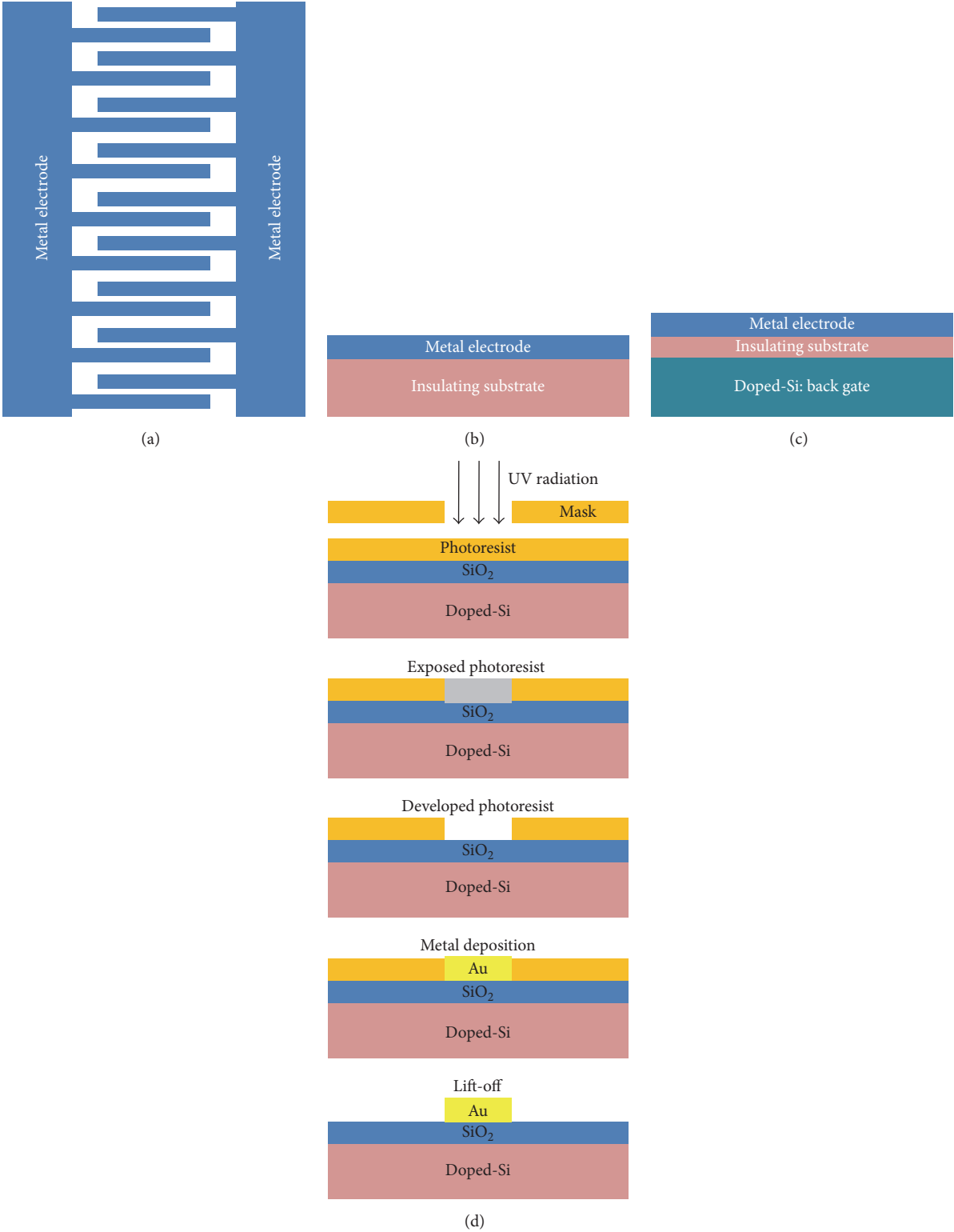SiO_2

Doped-Si

Lift-off

Au

SiO_2

Doped-Si

(d)

FIGURE 7: Schematic diagram of the metallic electrode structures. (a) Top view of the interdigitated structure. (b) Side view of substrate used for the two-point structure. (c) Side view of substrate used for the FET structure. (d) Steps of the photolithography process.
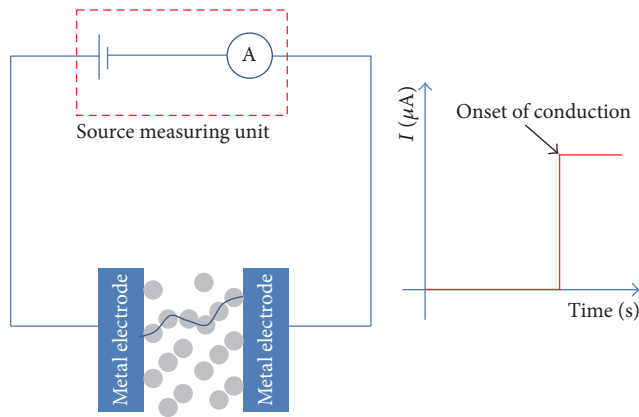
Figure 8: Schematic diagram of the onset of conduction measurement. The source measuring unit applies a voltage to the metallic electrodes and measures the electric current. A sharp rise in the electric current indicates the completion of at least one continuous network of nanoclusters between the contacts.

4. Progress in Conductometric Nanocluster Gas Sensors

Recently, highly stable and sensitive sensors have been made by incorporating various nanocluster materials into sensors [61–65]. Their novel fundamental phenomena and size dependent properties make them ideal candidates for the third-generation gas sensors. However, not all nanocluster materials are effective sensors. The selection of optimal sensing material is highly dependent on the design, manufacturing, chemical activity, stability, and so forth. In this section, research works recently published on the conductometric two-point and FET gas sensors that utilize nanoclusters will be reported.

Many types of nanoclusters were produced and tested with particular regard to their electrical properties in controlled atmosphere for gas sensing applications. Table 1 reports a list of the nanocluster gas sensors made of metal/metal-oxides that have been found in the literature together with the target gas(es) chosen. It is interesting to notice that tin oxide conductometric gas sensors are by far one of the most studied and also of the few that have been commercialized due to their better performances in terms of sensitivity and stability compared to other nanoclusters. Zinc oxide nanoclusters and nanowires are of the most studied [66–77]. This is due to the easiness of preparing nanoclusters/nanowires and multiple intriguing nanostructures and furthermore to the biocompatibility of zinc oxide that makes it promising for medical and in vivo applications. CuO is a striking p-type metal-oxide semiconductor that has unique optical, electrical, and catalytic properties [16]. Here, CuO nanoclusters would further endorse the chemical reactivity of the nanoclusters because as the surface-to-volume ratio of the particle increases, the number of reactive sites increases. This metal-oxide is known for its low cost and the antifouling effect which is effective for reducing the negative microorganisms [16]. Therefore, gas sensors of CuO nanoclusters can be used for implementable devices that are

Table 1: Nanocluster gas sensors made of metal/metal-oxides.

Year	Nanocluster	Target gas	Reference
2003	CeO_2	O_2	[80]
2004	Cu- and La-doped TiO_2	CO	[81]
2004	$SrTiO_3$	O_2	[82]
2004	Pd-Pt loaded SnO_2	CH_4	[83]
2004	SnO_2	O_2	[84]
2005	In-doped SnO_2	H_2, CH_4, C_3H_8	[85]
2005	ZnO doped with MnO_2, TiO_2 and Co_2O_3	Alcohol	[86]
2005	F-doped SnO_2	H_2, CO, CH_4, C_3H_8	[87]
2005	$SrTiO_3$	O_2	[88]
2005	$Ce_{1-x}Zr_xO_2$	O_2	[89]
2005	Pd and porous Si	H_2	[90]
2005	SnO_2	H_2	[91, 92]
2005	F-doped SnO_2	H_2	[93]
2005	$SrTiO_3$	O_2	[94]
2005	Scandia doped SnO_2	CO	[95]
2006	SnO_2	CO, O_2	[96]
2006	Cu-doped ZnO	CO	[97]
2006	$ZnFe_2O_4$	CH_3COHCH_3, C_2H_5OH	[98]
2006	$CoFe_2O_4$	Ethanol	[99]
2006	Pd-doped SnO_2	CO, O_2	[100]
2006	$TiO_2 : WO_3$	H_2	[101]
2006	Ba doped $SmCoO_3$	CO_2, O_2	[102]
2007	Al-doped TiO_2	CO	[103]
2007	Pd	H_2	[15]
2008	SnO_2/SBA-15	H_2	[104]
2008	SnO_2	O_2, CO, NO_2, H_2O	[105]
2009	SnO_2	H_2	[78]
2009	Pd and SnO_2 nanowires	H_2	[79]
2009	ZnO	H_2O	[106]
2009	Cu_2O and CuO	Acetone	[107]
2009	PdO-doped SnO_2	CO	[108]
2009	Y-doped TiO_2	CO	[109]
2009	Au-Pt	Methanol	[110]
2010	Pt and ZnO nanowires	Ethanol, NH_3	[111]
2011	Pd and Ag	H_2	[112]
2011	SnO_2	Ethanol, CH_3OH, C_2H_5OH	[113]
2011	Fe- and Co-doped HAp	CO	[114]
2012	SnO_2	CO	[115]
2013	Au and TiO_2	CO	[116]

TABLE 1: Continued.

Year	Nanocluster	Target gas	Reference
2013	ZnO	Ethanol	[117]
2014	Pd and VO	Ethanol	[118]
2014	Pd and SnO_2	H_2	[119]
2014	In_2O_3 and WO_3	H_2S	[120]
2014	Sm_2O_3 and ZnO	Ethanol	[121]
2014	SnO_2	Ethanol	[122]
2015	Pd/SnO_2	CO	[123]
2015	Au-Pt on GO	Uric acid and dopamine	[124]
2015	$Pt–SnO_2$	H_2, CO, and LPG	[125]
2015	Pt-graphene	H_2	[17]
2015	Au-Pd	H_2	[126]
2016	$CuFe_2O_4$	H_2	[127]
2016	CuO	H_2S	[16]
2016	α-iron oxide	Ethanol	[128]
2016	$In_4Sn_3O_{12}$ and TeO_2	CO	[129]
2016	Au@TiO_2	CO	[130]

biocompatible. In addition, palladium nanoclusters are of great importance for hydrogen sensing at room temperatures with optimal sensitivity and selectivity (this is important from safety point of view when dealing with explosive gases such as hydrogen). Therefore, this review will give special focus on some examples of those three nanoclusters: SnO_2, ZnO, CuO, Pd, Au, and Pt.

4.1. Tin Oxide Nanoclusters. Conductometric gas sensors based on SnO_2 nanoclusters that utilize the two-point structure were fabricated by Yeow et al. [78]. The nanoclusters were synthesized based on the hydrothermal method using potassium stannate trihydrate as a precursor in an ethanol-deionized water mixed solvent. The nanoclusters were diluted and dispersed in water before drop casting a few monolayers onto electrical electrodes. The response time is dependent on the operating temperature: 90% of resistance change (R_{air}-R_{gas}) was achieved within the first 1.3–3.0 min. A higher operating temperature leads to a greater change in conductance and, hence, greater response. On the other hand, desorption of all oxygen ionic species previously adsorbed occurs at high temperatures which explains the reduction in response as the operating temperature is increased beyond the optimum value. The results show none linear relationship of the response. A possible explanation of the response is that the inner surfaces of the porous nanocluster films are not fully utilized for gas detection due to the limitation of diffusion of the analyte gas through the nanopores.

The dependence of the gas sensor sensitivity on the size of nanoclusters used as a sensitive layer is a major factor controlling the performance of the gas sensor. As an example, Tan et al. have reported size dependence of the SnO_2 nanoclusters of sizes 20, 30, and 40 nm as shown in Figure 9 [14]. They showed that the sensor exhibits highly consistent

responses over many cycles, and the sensors made of smaller nanoclusters possess higher gas sensitivity due to the increase in effective surface area.

Shen et al. reported on two-point sensors that are based on SnO_2 nanowires which were synthesized by thermal evaporation at 900°C [79]. The nanowires were doped with palladium nanoclusters at 350°C for 30 min in air. Gas sensors based on SnO_2 nanowires with 0 wt%, 0.8 wt%, and 2 wt% Pd doping were fabricated. These gas sensors showed a reversible response to H_2 gas at an operating temperature of 150°C. The sensor response increased with Pd concentration. The 2 wt% Pd-doped SnO_2 nanowire sensor showed a response of two orders of magnitude for 1000 ppm H_2 gas at 100°C. Pd doping has demonstrated to improve the sensor response and lower the operating temperature.

4.2. Palladium Nanoclusters. Hydrogen gas sensors that utilize Pd nanoclusters with average sizes between 3.5 and 6 nm were reported by Van Lith et al. [15]. The nanoclusters were prepared by sputtering and inert gas condensation. The sensors are based on tunneling between discontinuous networks of nanoclusters. They demonstrated that the conduction through the nanocluster film is dominated by tunneling gaps; see Figure 10(a). The sensor operated at room temperature which make them usable for H_2 sensing safely. In addition, the sensor detected H_2 with concentration as low as 0.5% as depicted in Figure 10(b). The work showed that the sensor response is dependent on the nanocluster size (Figure 10(c)). The sensor resistance was found to decrease with increasing hydrogen concentration, a factor of ~10 at 5% of hydrogen; thus, the response is shown as the relative decrease in resistance ($\Delta R/R$). This was explained in terms of the increase in the nanocluster size upon exposure to H_2, thus decreasing the tunneling barriers which decrease the resistance of the sensor.

4.3. Copper Oxide Nanoclusters. H_2S gas sensors based on CuO nanoclusters are impeded in polymer membranes of poly-vinyl-alcohol (PVA) and glycerol ionic liquid (IL) [16]. The nanoclusters were fabricated with a precise control of nanoclusters size by the colloid microwave assisted hydrothermal method. Different concentrations of nanoclusters in polymer solutions of PVA and 5% IL were prepared. The solutions that contain nanoclusters were used to fabricate thin polymer membranes by the solution casting method, where the membranes hold semiconducting properties and were flexible. Each membrane was integrated between two electrical electrodes of capacitor structure as shown in the inset of Figure 11. Herein, the top and bottom electrodes were made of stainless steel grid and copper sheet, respectively. The conductance measurements revealed that those sensors were sensitive to H_2S gas with concentrations as low as 10 ppm, they are operational at low temperatures, and their sensing behavior was reversible which allowed multiple use of the produced sensors (see Figure 11). The produced sensors were also selective to H_2S, and they revealed reasonably fast response of 20.4 ± 12.8 s. The above sensors were reliable with low cost manufacturing; thus, they can be used for industrial field applications.
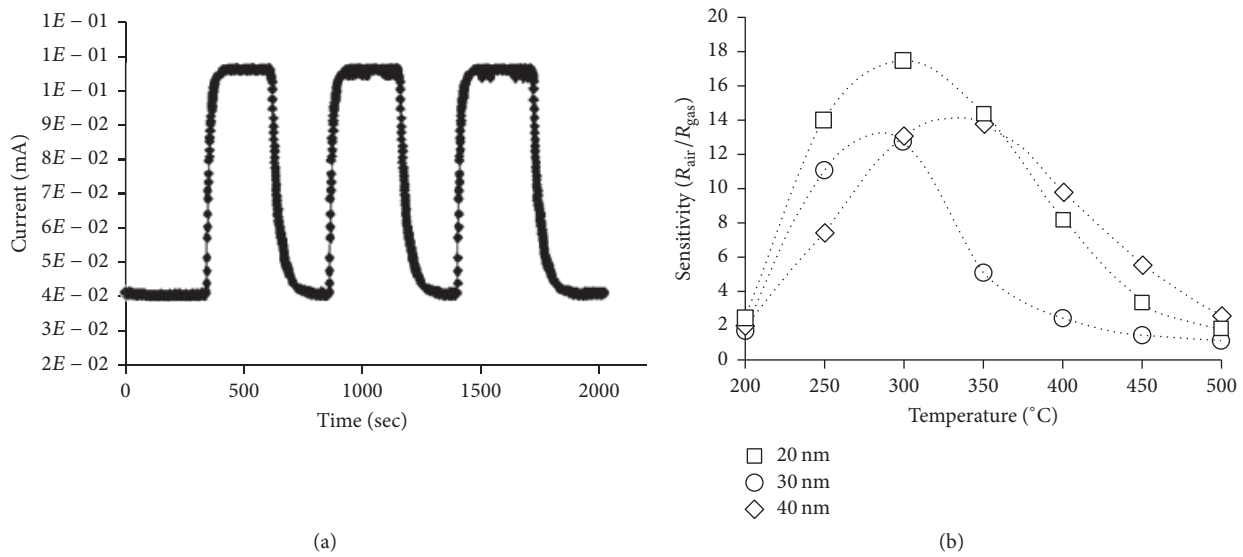
(a)

(b)

FIGURE 9: (a) Typical current response of a SnO$_2$ hydrogen sensor. (b) Sensitivity-temperature relationship before Pd functionalization. © IOP Publishing. Reproduced with permission. All rights reserved [14].
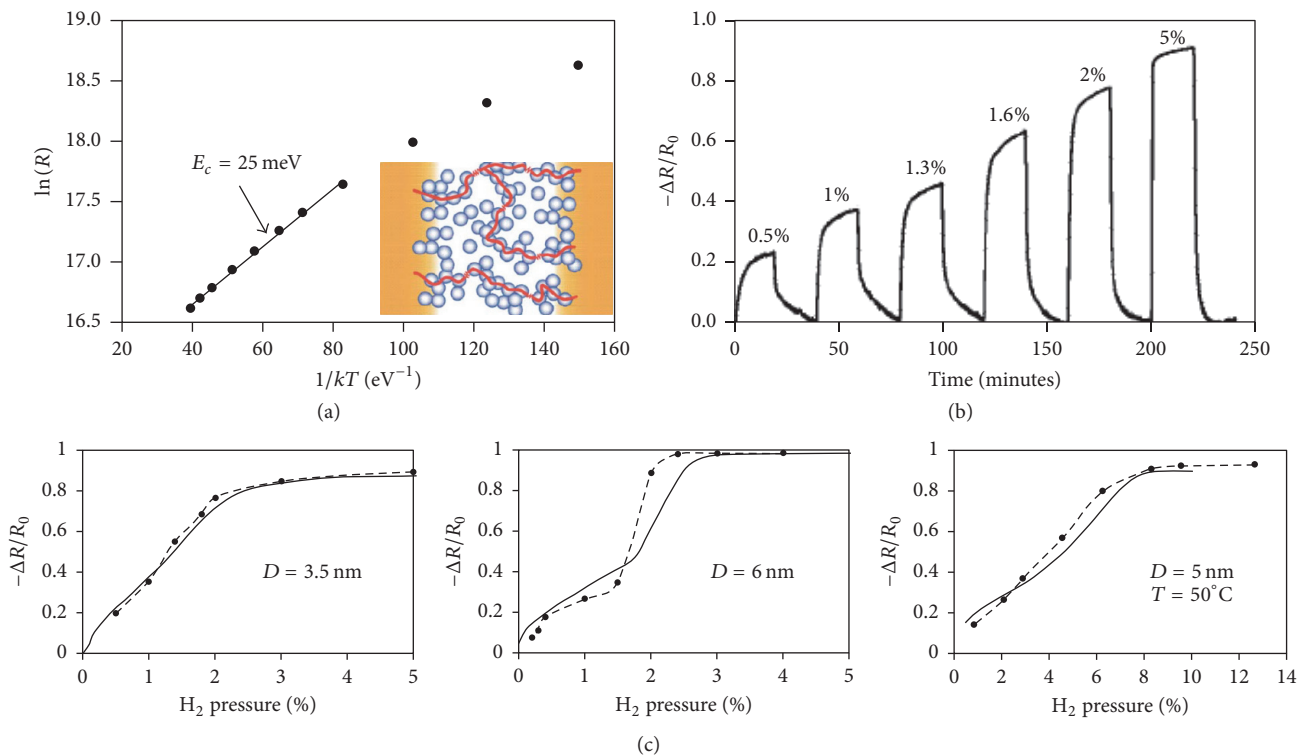

(a)

(b)

(c)

FIGURE 10: (a) Temperature dependence of the sensor resistance. The circles are experimental data and the line is a linear fit for activation energy of 25 meV. Inset: schematic illustration of a cluster film between two contacts. The main conduction paths are illustrated by the black lines, with tunnel gaps depicted by zigzag lines. (b) Transient response of a typical Pd cluster tunneling sensor to the hydrogen levels indicated. (c) Response at room temperature as a function of hydrogen pressure, given as the percentage of atmospheric pressure for 3.5 nm clusters and 6 nm nanoclusters. Response of a sensor fabricated with 5 nm clusters, measured at 50°C. The solid lines are experimental data, and the filled circles with dashed lines are theoretical fits. Reprinted with AIP permission from [15].
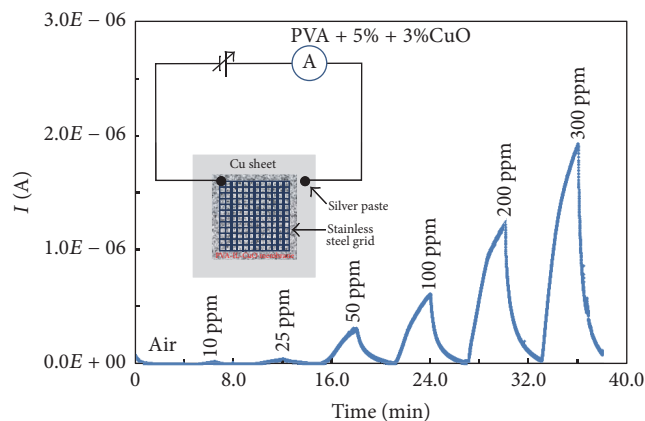
FIGURE 11: Electrical current response of PVA-IL-3%CuO sensor when exposed to H$_2$S gas with different concentrations measured at 80°C. The inset is a schematic diagram of the produced sensor and the electrical measurement circuit. Reprinted with Elsevier permission from [16].

4.4. Zinc Oxide Nanoclusters. ZnO nanoclusters were utilized for recognition of Chinese liquors by Zhang et al. [86]. The nanoclusters were prepared by the renovated hybrid induction and laser heating. The sensitivity of the sensor was enhanced by doping with MnO$_2$, TiO$_2$, and Co$_2$O$_3$. The doped nanoclusters were coated onto Al$_2$O$_3$ tubes (4 mm length, 1.2 mm external diameter, and 0.8 mm internal diameter) on which Pt electrodes had been fixed at each end. The thick films were sintered at 650°C for 2 hours after being dried under air to remove water. The film thickness observed by light microscopy was about 35 μm. A small Ni-Cr alloy coil with a resistance of about 33 Ω was placed through the tube as a heater. The sensors were tested against five different Chinese liquors, namely, Baiyunbian, Beijing Erguotou, Red Star Erguotou, Zhijiangdaqu, Jianliliangjiu, alcohol, and diluted alcohol (forged liquor). The significant sensitivity of each gas sensor to alcohol is obtained at about 320°C. It is shown that doping ZnO nanoclusters with MnO$_2$, TiO$_2$, and Co$_2$O$_3$ greatly improves the sensitivities to alcohol. Furthermore, they showed that the optimum operating temperature of the doped nano-ZnO gas sensors can be further reduced by suitable doping. The normalized principal component analysis (PCA) results of training data set projected onto their first two PCs have been proved to be effective for discriminating the response of gas sensor array to simple and complex odors. The PCA results depict that alcohol, diluted alcohol, and different flavor type liquors can be distinguished.

In a different work [106], ZnO nanostructure was prepared through the hydroxide precipitation using dropwise method and used to fabricate humidity sensors. The variations in resistance with the variations in humidity and temperature were tested. The curves for sensing element annealed at T = 150 and 300°C reveal that variation of resistance is slow in the region from 70% to 95%. However, the sample annealed at 450°C shows linearity in resistance versus %RH, which is suitable for device fabrication. Sensitivity curve for nanoclusters annealed at a temperature of 550°C

shows that, as RH increases, resistance decreases sharply up to 40% RH and shows highest sensitivity in this range; then it decreases less rapidly up to 95% RH as relative humidity increases. The sensing behavior was explained in terms of the adsorption of moisture which affects the protonic conduction on the surface and conductivity with varying amounts of water adsorbed by it. A hysteresis of sensing element versus humidity for sensing element prepared at 550°C was also observed. The sensing element shows less hysteresis (±5%) as compared to others. Curve "a" represents the values of resistance when %RH increases and curve "b" represents the values of resistances when %RH decreases. The response time of sensor is 80 sec for sensing element prepared at 550°C and this sensing element also shows repeatability within ±5% accuracy.

4.5. Gold and Platinum Nanoclusters. Au and Pt nanoclusters are commonly used as catalysts and sensors in many applications. Normally, either or both nanoclusters are integrated or alloyed with different nanomaterials to enhance their sensitivity and selectivity and to increase their kinetic oxygen reduction limitation [17, 124, 131]. Wang et al. fabricated hydrogen gas sensors using graphene oxide (GO) assembled with platinum (Pt) nanoclusters between a pair of prepatterned Ti/Au electrodes with microgap as shown in Figure 12 [17]. They assembled the nanomaterials by alternating current dielectrophoresis (DEP) method. The signal measurements for devices produced at different parameters that include processing time of a device, peak-to-peak voltage, and frequency were tested. The optimum sensing response of the device to hydrogen was at the measurement parameters of 5 V, 500 kHz, and 30 s, respectively. The fabricated device exhibits a sensitivity of (~10%) to 200 ppm hydrogen gas (measured using optimized parameters) at room temperature.

Recently, Liu et al. [124] synthesized nanocomposites of graphene oxide (GO) decorated with Au-Pt hybrid bimetallic nanoclusters with enhanced catalytic activity by an electrochemical reduction process on glassy carbon (ERGO) electrode. They investigated the synergistic electrocatalytic effect for electrodeposited bimetallic Au-Pt nanoclusters and GO utilized for detection of uric acid (UA) and dopamine (DA). The role of Au-Pt nanoclusters was to speed up the electron transfer for increasing the sensitivity while GO-ERGO allowed broader separation of the oxidation peak potentials for sensing DA and UA.

Conductometric hydrogen gas sensor based on Pt-SnO$_2$ nanoclusters was fabricated [125]. The results are that those sensors are sensitive to low hydrogen concentrations at sensor operating temperature of 85°C with response time of 0.5 s. Herein, Pt promotes dissociation of hydrogen molecules and activates reaction between adsorbed hydrogen and oxygen species on the surface of nanoclusters. The sensor was selective to hydrogen compared with CO and LPG (at 150 ppm) with the lowest response for LPG; thus, it can be used in hydrogen leak detection devices.

Lotus-like Au@TiO$_2$ nanoclusters were produced by hydrothermal reaction by controlling the ratio of Au to TiF$_4$ (without surfactant) [130]. The produced sensors were tested against O$_2$, H$_2$, NO, and CO. The best sensing performance
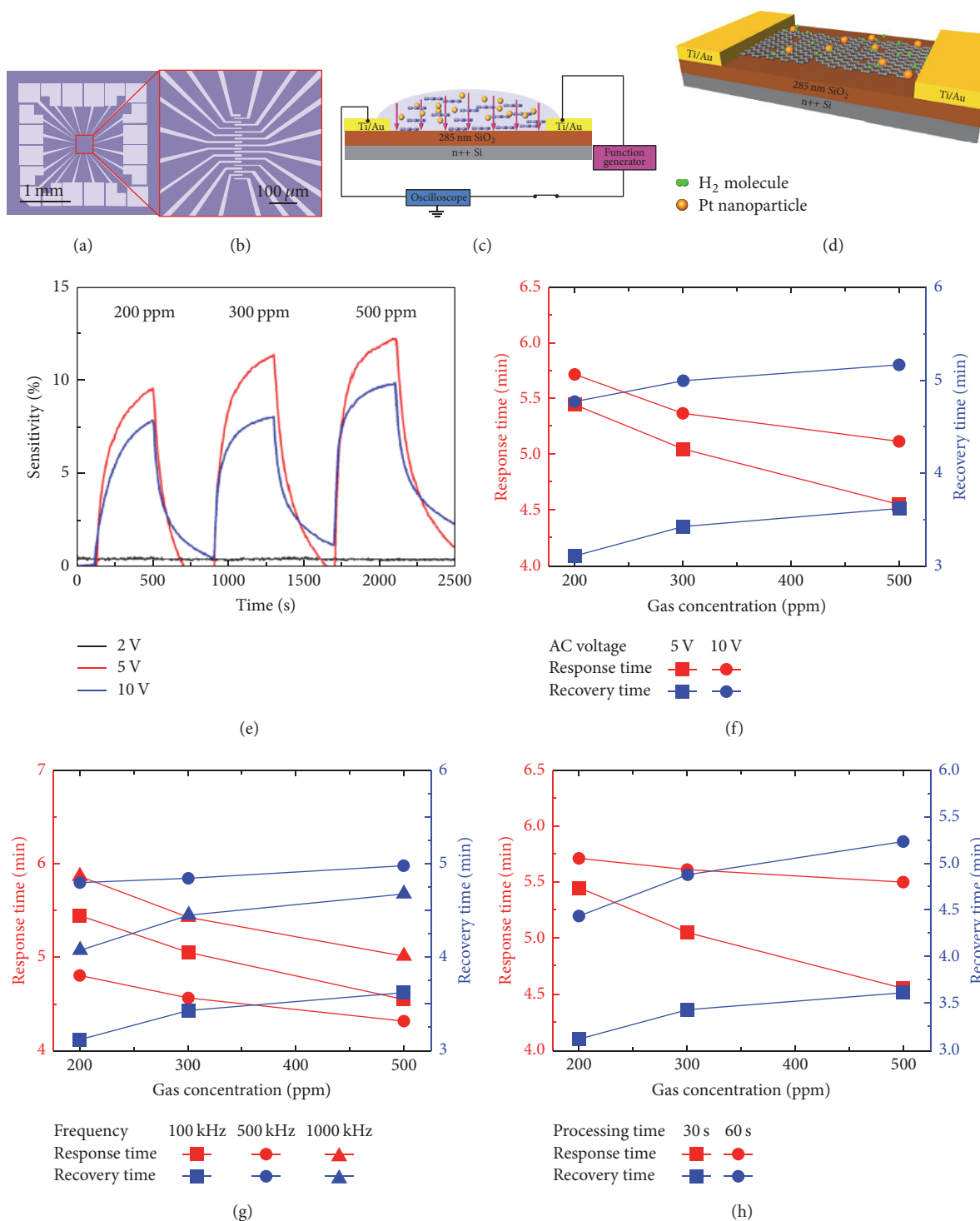
Figure 12: ((a) and (b)) Optical microscopy images of the prepatterned microgap electrodes. (c) Schematic diagram of DEP experiment. (d) Schematic diagram of the device. (e) Hydrogen gas response of the devices produced using 500 kHz frequency, 30 s processing time at various measurement voltages. (f)–(h) Response and recovery times of fabricated device at various voltage, frequency, and processing time, respectively. Reprinted with American Chemical Society permission from [17].

was for CO where the response rose to 17 for 500 ppm CO at 325°C, that is, 8.5 times better than that of pure TiO_2. Moreover, the selectivity, the response, and recovery time are improved greatly, which confirmed that the lotus-like

$Au@TiO_2$ nanostructures had promising potential in gas sensing applications. The enhancement in the sensing behavior was contributed to the catalytic activity of Au nanoclusters and unique lotus-like nanostructure.

Methanol sensor was developed using two porous Au electrodes with Pt nanoclusters that produces a micro/nano-porous Au-Pt system [110]. Each Au-Pt electrode acts as a current collector and gas diffusion layer for methanol. The sensor was fabricated by hot-pressing of the electrodes with Nafion film. The sensor showed response current in the temperature between 20 and 100°C for concentration of methanol between 0 and 2 M. The sensor has sensitivity of $9.6\,\text{mA/mM·cm}^2$ and a response time around 10 s with a sensor area of $0.25\,\text{cm}^2$.

5. Summary and Outlook

The article reviewed recent progress in gas sensors based on nanoclusters. During the past years, numerous new data on nanocluster gas sensor properties towards common target species such as H_2, O_2, and CO have been published. The use of nanoclusters allows the fabrication of an array of sensors in a chip with high sensitivity. The greater surface-to-volume ratio, the better stoichiometry, and greater level of crystallinity compared to bulk materials make the newly developed nanocluster gas sensors very promising for better understanding of sensing principles and development of a new generation of sensors. The selectivity of course remains a concern for metal and metal-oxide based gas sensor. This may be improved by fabricating sensor arrays using several different nanoclusters or by composite materials. The review focused on nanocluster production by inert gas condensation technique as a novel synthesis method. However, gas sensors based on nanoclusters synthesized by different methods were presented.

Nanocluster based sensors outperform their bulk component. There are still many parameters to be addressed. For commercial sensors, better control of the growth is required with a thorough understanding of the growth mechanism that can lead to a control in size distributions, shape, crystal structure, and atomic termination. In addition, attention has to be paid to issues like the electrical contacts and nanomanipulation that allow reliable production and integration of sensors. Other parameters such as limits of detection, limits of quantification, dynamic range, response and recovery times, and lifetime have to be improved. In addition, the drift of the sensors are frequently related to high working temperatures and exposure to chemically active ambient gas. In conclusion, future conductometric gas sensors should operate with multipurpose sensing and high selectivity recognition of specific chemical species. Sensors that are operated as standalone portable sensors are paramount for industrial applications.

Competing Interests

The author declares that there is no conflict of interests regarding the publication of this paper.

References

[1] Z. X. Cheng, X. H. Ren, J. Q. Xu, and Q. Y. Pan, "Mesoporous In$_2$O$_3$: effect of material structure on the gas sensing," *Journal of Nanomaterials*, vol. 2011, Article ID 654715, 6 pages, 2011.

[2] N. D. Hoa, N. V. Duy, S. A. El-Safty, and N. V. Hieu, "Meso-/nanoporous semiconducting metal oxides for gas sensor applications," *Journal of Nanomaterials*, vol. 2015, Article ID 972025, 14 pages, 2015.

[3] A. B. Kashyout, H. M. A. Soliman, H. Shokry Hassan, and A. M. Abousehly, "Fabrication of ZnO and ZnO:Sb Nanoparticles for gas sensor applications," *Journal of Nanomaterials*, vol. 2010, Article ID 341841, 8 pages, 2010.

[4] S. Semancik and R. E. Cavicchi, "The growth of thin, epitaxial SnO$_2$ films for gas sensing applications," *Thin Solid Films*, vol. 206, no. 1-2, pp. 81–87, 1991.

[5] N. S. Baik, G. Sakai, N. Miura, and N. Yamazoe, "Hydrothermally treated sol solution of tin oxide for thin-film gas sensor," *Sensors and Actuators B: Chemical*, vol. 63, no. 1, pp. 74–79, 2000.

[6] M. Ivanovskaya, P. Bogdanov, G. Faglia, and G. Sberveglieri, "Features of thin film and ceramic sensors at the detection of CO and NO2," *Sensors and Actuators B: Chemical*, vol. 68, no. 1, pp. 344–350, 2000.

[7] K. Ihokura and I. Watson, *The Stannic Oxide Gas Sensor—Principles and Applications*, CRC Press, Boca Raton, Fla, USA, 1994.

[8] W. Göpel and K. D. Schierbaum, "SnO2 sensors: current status and future prospects," *Sensors and Actuators: B. Chemical*, vol. 26, no. 1-3, pp. 1–12, 1995.

[9] G. Korotcenkov, "Practical aspects in design of one-electrode semiconductor gas sensors: status report," *Sensors and Actuators B: Chemical*, vol. 121, no. 2, pp. 664–678, 2007.

[10] N. Barsan and U. Weimar, "Conduction model of metal oxide gas sensors," *Journal of Electroceramics*, vol. 7, no. 3, pp. 143–167, 2001.

[11] N. Barsan and U. Weimar, "Understanding the fundamental principles of metal oxide based gas sensors; the example of CO sensing with SnO$_2$ sensors in the presence of humidity," *Journal of Physics: Condensed Matter*, vol. 15, no. 20, pp. R813–R839, 2003.

[12] A. I. Ayesh, S. Thaker, N. Qamhieh, and H. Ghamlouche, "Size-controlled Pd nanocluster grown by plasma gas-condensation method," *Journal of Nanoparticle Research*, vol. 13, no. 3, pp. 1125–1131, 2011.

[13] A. I. Ayesh, S. Thaker, N. Qamhieh, and H. Ghamlouche, "Investigation of the formation mechanisms of Pd nanoclusters produced using a magnetron sputtering source," *Advanced Materials Research*, vol. 324, pp. 145–148, 2011.

[14] E. T. H. Tan, G. W. Ho, A. S. W. Wong, S. Kawi, and A. T. S. Wee, "Gas sensing properties of tin oxide nanostructures synthesized via a solid-state reaction method," *Nanotechnology*, vol. 19, no. 25, Article ID 255706, 2008.

[15] J. Van Lith, A. Lassesson, S. A. Brown, M. Schulze, J. G. Partridge, and A. Ayesh, "A hydrogen sensor based on tunneling between palladium clusters," *Applied Physics Letters*, vol. 91, no. 18, Article ID 181910, 2007.

[16] A. I. Ayesh, A. F. S. Abu-Hani, S. T. Mahmou, and Y. Haik, "Selective H$_2$S sensor based on CuO nanoparticles embedded in organic membranes," *Sensors & Actuators B: Chemical*, vol. 231, pp. 593–600, 2016.

[17] J. Wang, S. Rathi, B. Singh, I. Lee, H.-I. Joh, and G.-H. Kim, "Alternating current dielectrophoresis optimization of Pt-decorated graphene oxide nanostructures for proficient hydrogen gas sensor," *ACS Applied Materials and Interfaces*, vol. 7, no. 25, pp. 13768–13775, 2015.

[18] N. Barsan, D. Koziej, and U. Weimar, "Metal oxide-based gas sensor research: how to?" *Sensors and Actuators B: Chemical*, vol. 121, no. 1, pp. 18–35, 2007.

[19] A. Chiorino, G. Ghiotti, F. Prinetto, M. C. Carotta, G. Martinelli, and M. Merli, "Characterization of SnO2-based gas sensors. A spectroscopic and electrical study of thick films from commercial and laboratory-prepared samples," *Sensors and Actuators B: Chemical*, vol. 44, no. 1-3, pp. 474–482, 1997.

[20] T. P. Hülser, H. Wiggers, F. E. Kruis, and A. Lorke, "Nanostructured gas sensors and electrical characterization of deposited SnO2 nanoparticles in ambient gas atmosphere," *Sensors and Actuators B: Chemical*, vol. 109, no. 1, pp. 13–18, 2005.

[21] M. Ramzan and R. Brydson, "Characterization of sub-stoichiometric tungsten trioxide (WO3-X) using impedance spectroscopy," *Sensors and Actuators A: Physical*, vol. 118, no. 2, pp. 322–331, 2005.

[22] A. Chandra Bose, P. Balaya, P. Thangadurai, and S. Ramasamy, "Grain size effect on the universality of AC conductivity in SnO2," *Journal of Physics and Chemistry of Solids*, vol. 64, no. 4, pp. 659–663, 2003.

[23] G. Martinelli, M. C. Carotta, L. Passari, and L. Tracchi, "A study of the moisture effects on SnO2 thick films by sensitivity and permittivity measurements," *Sensors and Actuators: B. Chemical*, vol. 26, no. 1-3, pp. 53–55, 1995.

[24] G. Ghiotti, A. Chiorino, G. Martinelli, and M. C. Carotta, "Moisture effects on pure and Pd-doped SnO2 thick films analysed by FTIR spectroscopy and conductance measurements," *Sensors and Actuators: B. Chemical*, vol. 25, no. 1-3, pp. 520–524, 1995.

[25] A. Labidi, C. Jacolin, M. Bendahan et al., "Impedance spectroscopy on WO3 gas sensor," *Sensors and Actuators, B: Chemical*, vol. 106, no. 2, pp. 713–718, 2005.

[26] L. Chen and S. C. Tsang, "Ag doped WO3-based powder sensor for the detection of NO gas in air," *Sensors and Actuators, B: Chemical*, vol. 89, no. 1-2, pp. 68–75, 2003.

[27] P. Montmeat, R. Lalauze, J.-P. Viricelle, G. Tournier, and C. Pijolat, "Model of the thickness effect of SnO2 thick film on the detection properties," *Sensors and Actuators, B: Chemical*, vol. 103, no. 1-2, pp. 84–90, 2004.

[28] M. Hausner, J. Zacheja, and J. Binder, "Multi-electrode substrate for selectivity enhancement in air monitoring," *Sensors and Actuators, B: Chemical*, vol. 43, no. 1-3, pp. 11–17, 1997.

[29] F. Hossein-Babaei and M. Orvatinia, "Analysis of thickness dependence of the sensitivity in thin film resistive gas sensors," *Sensors and Actuators, B: Chemical*, vol. 89, no. 3, pp. 256–261, 2003.

[30] S.-S. Park and J. D. Mackenzie, "Thickness and microstructure effects on alcohol sensing of tin oxide thin films," *Thin Solid Films*, vol. 274, no. 1-2, pp. 154–159, 1996.

[31] S. M. A. Durrani, E. E. Khawaja, and M. F. Al-Kuhaili, "CO-sensing properties of undoped and doped tin oxide thin films prepared by electron beam evaporation," *Talanta*, vol. 65, no. 5, pp. 1162–1167, 2005.

[32] G. G. Mandayo, E. Castaño, F. J. Gracia, A. Cirera, A. Cornet, and J. R. Morante, "Strategies to enhance the carbon monoxide sensitivity of tin oxide thin films," *Sensors and Actuators, B: Chemical*, vol. 95, no. 1-3, pp. 90–96, 2003.

[33] X. Vilanova, E. Llobet, J. Brezmes, J. Calderer, and X. Correig, "Numerical simulation of the electrode geometry and position effects on semiconductor gas sensor response," *Sensors and Actuators, B: Chemical*, vol. 48, no. 1-3, pp. 425–431, 1998.

[34] D. E. Williams and K. F. E. Pratt, "Theory of self-diagnostic sensor array devices using gas-sensitive resistors," *Journal of the Chemical Society, Faraday Transactions*, vol. 91, no. 13, pp. 1961–1966, 1995.

[35] K. Kalantar-zadeh and B. Fry, *Nanotechnology Enabled Sensors*, Springer, Berlin, Germany, 2008.

[36] A. N. Shipway, E. Katz, and I. Willner, "Nanoparticle arrays on surfaces for electronic, optical, and sensor applications," *ChemPhysChem*, vol. 1, no. 1, pp. 18–52, 2000.

[37] M. Lai and D. J. Riley, "Templated electrosynthesis of nanomaterials and porous structures," *Journal of Colloid and Interface Science*, vol. 323, no. 2, pp. 203–212, 2008.

[38] A. Jaworek, "Micro- and nanoparticle production by electrospraying," *Powder Technology*, vol. 176, no. 1, pp. 18–35, 2007.

[39] D. G. Shchukin and G. B. Sukhorukov, "Nanoparticle synthesis in engineered organic nanoscale reactors," *Advanced Materials*, vol. 16, no. 8, pp. 671–682, 2004.

[40] J. A. Gerbec, D. Magana, A. Washington, and G. F. Strouse, "Microwave-enhanced reaction rates for nanoparticle synthesis," *Journal of the American Chemical Society*, vol. 127, no. 45, pp. 15791–15800, 2005.

[41] B. Xia, I. W. Lenggoro, and K. Okuyama, "Novel route to nanoparticle synthesis by salt-assisted aerosol decomposition," *Advanced Materials*, vol. 13, no. 20, pp. 1579–1582, 2001.

[42] C. Binns, "Nanoclusters deposited on surfaces," *Surface Science Reports*, vol. 44, no. 1-2, pp. 1–49, 2001.

[43] F. Baletto and R. Ferrando, "The surface of helium crystals," *Reviews of Modern Physics*, vol. 77, no. 1, p. 317, 2005.

[44] A. Banerjee and B. Das, "An ultrahigh vacuum complementary metal oxide silicon compatible nonlithographic system to fabricate nanoparticle-based devices," *Review of Scientific Instruments*, vol. 79, no. 3, Article ID 033910, 2008.

[45] E. Pérez-Tijerina, S. Mejía-Rosales, H. Inada, and M. José-Yacamán, "Effect of temperature on AuPd nanoparticles produced by inert gas condensation," *Journal of Physical Chemistry C*, vol. 114, no. 15, pp. 6999–7003, 2010.

[46] W. A. de Heer, "The physics of simple metal clusters: experimental aspects and simple models," *Reviews of Modern Physics*, vol. 65, no. 3, article 611, 1993.

[47] H. Haberland, US Patent No. 5110435, 1992.

[48] S. Pratontep, S. J. Carroll, C. Xirouchaki, M. Streun, and R. E. Palmer, "Size-selected cluster beam source based on radio frequency magnetron plasma sputtering and gas condensation," *Review of Scientific Instruments*, vol. 76, no. 4, Article ID 045103, 2005.

[49] A. I. Ayesh, N. Qamhieh, H. Ghamlouche, S. Thaker, and M. El-Shaer, "Fabrication of size-selected Pd nanoclusters using a magnetron plasma sputtering source," *Journal of Applied Physics*, vol. 107, no. 3, Article ID 034317, 2010.

[50] A. I. Ayesh, "Electronic transport in Pd nanocluster devices," *Applied Physics Letters*, vol. 98, no. 13, Article ID 133108, 2011.

[51] J. Schmelzer Jr., S. A. Brown, A. Wurl, M. Hyslop, and R. J. Blaikie, "Finite-size effects in the conductivity of cluster assembled nanostructures," *Physical Review Letters*, vol. 88, no. 22, Article ID 226802, 2002.

[52] A. I. Ayesh, N. Qamhieh, S. T. Mahmoud, and H. Alawadhi, "Production of size-selected Cu_xSn_{1-x} nanoclusters," *Advanced Materials Research*, vol. 295–297, pp. 70–73, 2011.

[53] A. I. Ayesh, H. A. Ahmed, F. Awwad, S. I. Abu-Eishah, and S. T. Mahmood, "Mechanisms of Ti nanocluster formation by inert

gas condensation," *Journal of Materials Research*, vol. 28, no. 18, pp. 2622–2628, 2013.

[54] M. Ohring, *Materials Science of Thin Films*, Academic Press, Cambridge, Mass, USA, 2nd edition, 2002.

[55] J. B. Chen, J. F. Zhou, A. Hafele et al., "Morphological studies of nanostructures from directed cluster beam deposition," *The European Physical Journal D*, vol. 34, no. 1, pp. 251–254, 2005.

[56] O. Kamalou, J. Rangama, J.-M. Ramillon, P. Guinement, and B. A. Huber, "Production of pulsed, mass-selected beams of metal and semiconductor clusters," *Review of Scientific Instruments*, vol. 79, no. 6, Article ID 063301, 2008.

[57] A. N. Banerjee, R. Krishna, and B. Das, "Size controlled deposition of Cu and Si nano-clusters by an ultra-high vacuum sputtering gas aggregation technique," *Applied Physics A*, vol. 90, pp. 299–303, 2008.

[58] A. I. Ayesh, N. Qamhieh, S. T. Mahmoud, and H. Alawadhi, "Fabrication of size-selected bimetallic nanoclusters using magnetron sputtering," *Journal of Materials Research*, vol. 27, no. 18, pp. 2441–2446, 2012.

[59] P. H. Dawson, *Quadrupole Mass Spectrometry and Its Applications*, Elsevier Press, Amsterdam, The Netherlands, 1976.

[60] W. J. Liu, J. Zhang, L. J. Wan et al., "Dielectrophoretic manipulation of nano-materials and its application to micro/nanosensors," *Sensors and Actuators, B: Chemical*, vol. 133, no. 2, pp. 664–670, 2008.

[61] N. Pinna, G. Neri, M. Antonietti, and M. Niederberger, "Nonaqueous synthesis of nanocrystalline semiconducting metal oxides for gas sensing," *Angewandte Chemie—International Edition*, vol. 43, no. 33, pp. 4345–4349, 2004.

[62] L. P. Sun, L. H. Huo, H. Zhao, S. Gao, and J. G. Zhao, "Preparation and gas-sensing property of a nanosized titania thin film towards alcohol gases," *Sensors and Actuators B: Chemical*, vol. 114, no. 1, pp. 387–391, 2006.

[63] Z. Liu, T. Yamazaki, Y. Shen, T. Kikuta, N. Nakatani, and Y. Li, "O2 and CO sensing of Ga2O3 multiple nanowire gas sensors," *Sensors and Actuators, B: Chemical*, vol. 129, no. 2, pp. 666–670, 2008.

[64] C. S. Rout, A. R. Raju, A. Govindaraj, and C. N. R. Rao, "Ethanol and hydrogen sensors based on ZnO nanoparticles and nanowires," *Journal of Nanoscience and Nanotechnology*, vol. 7, no. 6, pp. 1923–1929, 2007.

[65] M. S. Arnold, P. Avouris, Z. W. Pan, and Z. L. Wang, "Field-effect transistors based on single semiconducting oxide nanobelts," *Journal of Physical Chemistry B*, vol. 107, no. 3, pp. 659–663, 2003.

[66] J. Zhong, S. Muthukumar, Y. Chen et al., "Ga-doped ZnO single-crystal nanotips grown on fused silica by metalorganic chemical vapor deposition," *Applied Physics Letters*, vol. 83, no. 16, p. 3401, 2003.

[67] S. Y. Bae, C. W. Na, J. H. Kang, and J. Park, "Comparative structure and optical properties of Ga-, In-, and Sn-doped ZnO nanowires synthesized via thermal evaporation," *The Journal of Physical Chemistry B*, vol. 109, no. 7, pp. 2526–2531, 2005.

[68] S. Y. Li, P. Lin, C. Y. Lee, T. Y. Tseng, and C. J. Huang, "Effect of Sn dopant on the properties of ZnO nanowires," *Journal of Physics D: Applied Physics*, vol. 37, no. 16, p. 2274, 2004.

[69] D. K. Hwang, H. S. Kim, J. H. Lim et al., "Study of the photoluminescence of phosphorus-doped *p*-type ZnO thin films grown by radio-frequency magnetron sputtering," *Applied Physics Letters*, vol. 86, no. 15, Article ID 151917, 2005.

[70] W. Lee, M.-C. Jeong, S.-W. Joo, and J.-M. Myoung, "Arsenic doping of ZnO nanowires by post-annealing treatment," *Nanotechnology*, vol. 16, no. 6, pp. 764–768, 2005.

[71] W. Lee, M. C. Jeong, and J. M. Myoung, "Optical characteristics of arsenic-doped ZnO nanowires," *Applied Physics Letters*, vol. 85, no. 25, article 6167, 2004.

[72] D. W. Zeng, C. S. Xie, B. L. Zhu et al., "Controlled growth of ZnO nanomaterials via doping Sb," *Journal of Crystal Growth*, vol. 266, no. 4, pp. 511–518, 2004.

[73] G. Shen, J. H. Cho, J. K. Yoo, G.-C. Yi, and C. J. Lee, "Synthesis and optical properties of S-doped ZnO nanostructures: nanonails and nanowires," *Journal of Physical Chemistry B*, vol. 109, no. 12, pp. 5491–5496, 2005.

[74] J. B. Cui and U. J. Gibson, "Electrodeposition and room temperature ferromagnetic anisotropy of Co and Ni-doped ZnO nanowire arrays," *Applied Physics Letters*, vol. 87, no. 13, Article ID 133108, 2005.

[75] C. X. Xu, X. W. Sun, Z. L. Dong, M. B. Yu, Y. Z. Xiong, and J. S. Chen, "Magnetic nanobelts of iron-doped zinc oxide," *Applied Physics Letters*, vol. 86, no. 17, Article ID 173110, 2005.

[76] D. A. Schwartz, K. R. Kittilstved, and D. R. Gamelin, "Above-room-temperature ferromagnetic Ni^{2+}-doped ZnO thin films prepared from colloidal diluted magnetic semiconductor quantum dots," *Applied Physics Letters*, vol. 85, no. 8, pp. 1395–1397, 2004.

[77] C. Ronning, P. X. Gao, Y. Ding, Z. L. Wang, and D. Schwen, "Manganese-doped ZnO nanobelts for spintronics," *Applied Physics Letters*, vol. 84, no. 5, pp. 783–785, 2004.

[78] S. C. Yeow, W. L. Ong, A. S. W. Wong, and G. W. Ho, "Template-free synthesis and gas sensing properties of well-controlled porous tin oxide nanospheres," *Sensors and Actuators B: Chemical*, vol. 143, no. 1, pp. 295–301, 2009.

[79] Y. Shen, T. Yamazaki, Z. Liu et al., "Microstructure and H2 gas sensing properties of undoped and Pd-doped SnO2 nanowires," *Sensors and Actuators, B: Chemical*, vol. 135, no. 2, pp. 524–529, 2009.

[80] N. Izu, W. Shin, and N. Murayama, "Fast response of resistive-type oxygen gas sensors based on nano-sized ceria powder," *Sensors and Actuators, B: Chemical*, vol. 93, no. 1-3, pp. 449–453, 2003.

[81] A. M. Ruiz, A. Cornet, and J. R. Morante, "Study of La and Cu influence on the growth inhibition and phase transformation of nano-TiO2 used for gas sensors," *Sensors and Actuators, B: Chemical*, vol. 100, no. 1-2, pp. 256–260, 2004.

[82] Y. Hu, O. K. Tan, W. Cao, and W. Zhu, "A low temperature nano-structured SrTiO3 thick film oxygen gas sensor," *Ceramics International*, vol. 30, no. 7, pp. 1819–1822, 2004.

[83] S.-J. Hong and J.-I. Han, "Effect of low temperature composite catalyst loading (LTC2L) on sensing properties of nano gas sensor," *Sensors and Actuators, A: Physical*, vol. 112, no. 1, pp. 80–86, 2004.

[84] T. G. G. Maffeis, M. Penny, K. S. Teng, S. P. Wilks, H. S. Ferkel, and G. T. Owen, "Macroscopic and microscopic investigations of the effect of gas exposure on nanocrystalline SnO$_2$ at elevated temperature," *Applied Surface Science*, vol. 234, no. 1–4, pp. 82–85, 2004.

[85] K. S. Yoo, S. H. Park, and J. H. Kang, "Nano-grained thin-film indium tin oxide gas sensors for H$_2$ detection," *Sensors and Actuators B: Chemical*, vol. 108, no. 1-2, pp. 159–164, 2005.

[86] Q. Zhang, C. Xie, S. Zhang et al., "Identification and pattern recognition analysis of Chinese liquors by doped nano ZnO gas

sensor array," *Sensors and Actuators, B: Chemical*, vol. 110, no. 2, pp. 370–376, 2005.

[87] C.-H. Han, S.-D. Han, I. Singh, and T. Toupance, "Micro-bead of nano-crystalline F-doped SnO2 as a sensitive hydrogen gas sensor," *Sensors and Actuators, B: Chemical*, vol. 109, no. 2, pp. 264–269, 2005.

[88] C. Xiangfeng, J. Dongli, G. Yu, and Z. Chenmou, "Ethanol gas sensor based on CoFe2O4 nano-crystallines prepared by hydrothermal method," *Sensors and Actuators, B: Chemical*, vol. 120, no. 1, pp. 177–181, 2006.

[89] N. Izu, N. Oh-Hori, M. Itou, W. Shin, I. Matsubara, and N. Murayama, "Resistive oxygen gas sensors based on $Ce_{1-x}Zr_xO_2$ nano powder prepared using new precipitation method," *Sensors and Actuators, B: Chemical*, vol. 108, no. 1-2, pp. 238–243, 2005.

[90] K. Luongo, A. Sine, and S. Bhansali, "Development of a highly sensitive porous Si-based hydrogen sensor using Pd nano-structures," *Sensors and Actuators B: Chemical*, vol. 111-112, pp. 125–129, 2005.

[91] S. Shukla, R. Agrawal, H. J. Cho, and S. Seal, "Effect of ultraviolet radiation exposure on room-temperature hydrogen sensitivity of nanocrystalline doped tin oxide sensor incorporated into microelectromechanical systems device," *Journal of Applied Physics*, vol. 97, no. 5, Article ID 054307, 2005.

[92] S. P. Zhang, H. J. Cho, Z. Rahman, C. Drake, and S. Seal, "Hydrogen-discriminating nanocrystalline doped-tin-oxide room-temperature microsensor," *Journal of Applied Physics*, vol. 98, no. 10, Article ID 104306, 2005.

[93] C.-H. Han, S.-D. Han, I. Singh, and T. Toupance, "Micro-bead of nano-crystalline F-doped SnO_2 as a sensitive hydrogen gas sensor," *Sensors and Actuators B: Chemical*, vol. 109, no. 2, pp. 264–269, 2005.

[94] Y. Hu, O. K. Tan, J. S. Pan, H. Huang, and W. Cao, "The effects of annealing temperature on the sensing properties of low temperature nano-sized $SrTiO_3$ oxygen gas sensor," *Sensors and Actuators B: Chemical*, vol. 108, no. 1-2, pp. 244–249, 2005.

[95] G. Xu, Y.-W. Zhang, X. Sun, C.-L. Xu, and C.-H. Yan, "Synthesis, structure, texture, and CO sensing behavior of nanocrystalline tin oxide doped with scandia," *The Journal of Physical Chemistry B*, vol. 109, no. 8, pp. 3269–3278, 2005.

[96] J. C. Belmonte, J. Manzano, J. Arbiol et al., "Micromachined twin gas sensor for CO and O_2 quantification based on catalytically modified nano-SnO_2," *Sensors and Actuators, B: Chemical*, vol. 114, no. 2, pp. 881–892, 2006.

[97] H. Gong, J. Q. Hu, J. H. Wang, C. H. Ong, and F. R. Zhu, "Nano-crystalline Cu-doped ZnO thin film gas sensor for CO," *Sensors and Actuators, B: Chemical*, vol. 115, no. 1, pp. 247–251, 2006.

[98] X. Chu, D. Jiang, and C. Zheng, "The gas-sensing properties of thick film sensors based on nano-$ZnFe_2O_4$ prepared by hydrothermal method," *Materials Science and Engineering: B*, vol. 129, no. 1-3, pp. 150–153, 2006.

[99] Y. Hu, O. K. Tan, J. S. Pan, H. Huang, and W. Cao, "The effects of annealing temperature on the sensing properties of low temperature nano-sized SrTiO3 oxygen gas sensor," *Sensors and Actuators, B: Chemical*, vol. 108, no. 1-2, pp. 244–249, 2005.

[100] J. Cerdà Belmonte, J. Manzano, J. Arbiol et al., "Micromachined twin gas sensor for CO and O_2 quantification based on catalytically modified nano-SnO_2," *Sensors and Actuators B: Chemical*, vol. 114, no. 2, pp. 881–892, 2006.

[101] G. N. Chaudhari, A. M. Bende, A. B. Bodade, S. S. Patil, and V. S. Sapkal, "Structural and gas sensing properties of nanocrystalline TiO2:WO3-based hydrogen sensors," *Sensors and Actuators, B: Chemical*, vol. 115, no. 1, pp. 297–302, 2006.

[102] E. Delgado and C. R. Michel, "CO_2 and O_2 sensing behavior of nanostructured barium-doped $SmCoO_3$," *Materials Letters*, vol. 60, no. 13-14, pp. 1613–1616, 2006.

[103] Y. J. Choi, Z. Seeley, A. Bandyopadhyay, S. Bose, and S. A. Akbar, "Aluminum-doped TiO2 nano-powders for gas sensors," *Sensors and Actuators, B: Chemical*, vol. 124, no. 1, pp. 111–117, 2007.

[104] J. Yang, K. Hidajat, and S. Kawi, "Synthesis of nano-SnO2/SBA-15 composite as a highly sensitive semiconductor oxide gas sensor," *Materials Letters*, vol. 62, no. 8-9, pp. 1441–1443, 2008.

[105] S. Palzer, E. Moretton, F. H. Ramirez, A. Romano-Rodriguez, and J. Wöllenstein, "Nano- and microsized metal oxide thin film gas sensors," *Microsystem Technologies*, vol. 14, no. 4-5, pp. 645–651, 2008.

[106] B. C. Yadav, R. Srivastava, C. D. Dwivedi, and P. Pramanik, "Synthesis of nano-sized ZnO using drop wise method and its performance as moisture sensor," *Sensors and Actuators, A: Physical*, vol. 153, no. 2, pp. 137–141, 2009.

[107] E. Comini, G. Sberveglieri, C. Sada et al., "Chemical vapor deposition of Cu2O and CuO nanosystems for innovative gas sensors," in *Proceedings of the IEEE Sensors 2009 Conference (SENSORS'09)*, pp. 111–113, October 2009.

[108] M. Yuasa, T. Masaki, T. Kida, K. Shimanoe, and N. Yamazoe, "Nano-sized PdO loaded SnO_2 nanoparticles by reverse micelle method for highly sensitive CO gas sensor," *Sensors and Actuators B: Chemical*, vol. 136, no. 1, pp. 99–104, 2009.

[109] Z. Seeley, Y. J. Choi, and S. Bose, "Citrate-nitrate synthesis of nano-structured titanium dioxide ceramics for gas sensors," *Sensors and Actuators B: Chemical*, vol. 140, no. 1, pp. 98–103, 2009.

[110] J. D. Kim, Y. J. Lee, and J. Y. Park, "Extremely small methanol sensor with micro/nano porous Au-Pt electrodes for compact DMFC applications," in *Proceedings of the IEEE SENSORS Conference*, pp. 1943–1946, 2009.

[111] S. J. Chang, W. Y. Weng, C. L. Hsu, and T. J. Hsueh, "High sensitivity of a ZnO nanowire-based ammonia gas sensor with Pt nano-particles," *Nano Communication Networks*, vol. 1, no. 4, pp. 283–288, 2010.

[112] R. Dasari, F. J. Ibañez, and F. P. Zamborini, "Electrochemical fabrication of metal/organic/metal junctions for molecular electronics and sensing applications," *Langmuir*, vol. 27, no. 11, pp. 7285–7293, 2011.

[113] L. Mahdavian, "Thermodynamic study of alcohol on SnO2 (100)-based gas nano-sensor," *Physics and Chemistry of Liquids*, vol. 49, no. 5, pp. 626–638, 2011.

[114] R. Khairnar, R. Mene, S. Munde, and M. Mahabole, "Nano-hydroxyapatite thick film gas sensors," in *Proceedings of the 4th Nanoscience and Nanotechnolgy sSymposium (NNS '11)*, vol. 1415 of *AIP Conference Proceedings*, pp. 189–192, Bali, Indonesia, December 2011.

[115] M. A. Andio, P. N. Browning, P. A. Morris, and S. A. Akbar, "Comparison of gas sensor performance of SnO_2 nano-structures on microhotplate platforms," *Sensors and Actuators, B: Chemical*, vol. 165, no. 1, pp. 13–18, 2012.

[116] Y.-S. Kim, P. Rai, and Y.-T. Yu, "Microwave assisted hydrothermal synthesis of Au@TiO2 core-shell nanoparticles for high temperature CO sensing applications," *Sensors and Actuators, B: Chemical*, vol. 186, pp. 633–639, 2013.

[117] N. J. Ridha, M. H. H. Jumali, A. A. Umar, and F. K. Mohamad, "Ethanol sensor based on ZnO nanostructures prepared via microwave oven," in *Proceedings of the 7th International Conference on Sensing Technology (ICST '13)*, pp. 121–126, Wellington, New Zealand, December 2013.

[118] W. Jin, S. Yan, W. Chen, S. Yang, C. Zhao, and Y. Dai, "Enhanced ethanol sensing characteristics by decorating dispersed Pd nanoparticles on vanadium oxide nanotubes," *Materials Letters*, vol. 128, pp. 362–365, 2014.

[119] A. I. Ayesh, S. T. Mahmoud, S. J. Ahmad, and Y. Haik, "Novel hydrogen gas sensor based on Pd and SnO2 nanoclusters," *Materials Letters*, vol. 128, pp. 354–357, 2014.

[120] L. Yin, D. Chen, M. Hu et al., "Microwave-assisted growth of In2O3 nanoparticles on WO3 nanoplates to improve H2S-sensing performance," *Journal of Materials Chemistry A*, vol. 2, no. 44, pp. 18867–18874, 2014.

[121] M. Bagheri, N. F. Hamedani, A. R. Mahjoub, A. A. Khodadadi, and Y. Mortazavi, "Highly sensitive and selective ethanol sensor based on Sm2O3-loaded flower-like ZnO nanostructure," *Sensors and Actuators, B: Chemical*, vol. 191, pp. 283–290, 2014.

[122] N. Rajesha, J. C. Kannanb, T. Krishnakumar, S. G. Leonardidid, and G. Neri, "Sensing behavior to ethanol of tin oxide nanoparticles prepared by microwave synthesis with different irradiation time," *Sensors and Actuators B: Chemical*, vol. 194, pp. 96–104, 2014.

[123] Q. Wang, C. Wang, H. Sun et al., "Microwave assisted synthesis of hierarchical Pd/SnO$_2$ nanostructures for CO gas sensor," *Sensors and Actuators, B: Chemical*, vol. 222, Article ID 18846, pp. 257–263, 2016.

[124] Y. Liu, P. She, J. Gong et al., "A novel sensor based on electrodeposited Au–Pt bimetallic nano-clusters decorated on graphene oxide (GO)-electrochemically reduced GO for sensitive detection of dopamine and uric acid," *Sensors and Actuators B*, vol. 221, pp. 1542–1553, 2015.

[125] S. Rane, S. Arbuj, S. Rane, and S. Gosavi, "Hydrogen sensing characteristics of Pt-SnO$_2$ nano-structured composite thin films," *Journal of Materials Science: Materials in Electronics*, vol. 26, no. 6, pp. 3707–3716, 2015.

[126] C. Wadell, F. A. A. Nugroho, E. Lidström, B. Iandolo, J. B. Wagner, and C. Langhammer, "Hysteresis-free nanoplasmonic pd-au alloy hydrogen sensors," *Nano Letters*, vol. 15, no. 5, pp. 3563–3570, 2015.

[127] M. A. Haija, A. I. Ayesh, S. Ahmed, and M. S. Katsiotis, "Selective hydrogen gas sensor using CuFe2O4 nanoparticle based thin film," *Applied Surface Science*, vol. 369, pp. 443–447, 2016.

[128] S. G. Leonardi, A. Mirzaei, A. Bonavita et al., "A comparison of the ethanol sensing properties of -iron oxide nanostructures prepared via the sol-gel and electrospinning techniques," *Nanotechnology*, vol. 27, no. 7, Article ID 075502, 2016.

[129] A. Mirzaei, S. Park, G.-J. Sun, H. Kheel, and C. Lee, "CO gas sensing properties of In$_4$Sn$_3$O$_{12}$ and TeO$_2$ composite nanoparticle sensors," *Journal of Hazardous Materials*, vol. 305, pp. 130–138, 2016.

[130] H. Liu, W. Yang, M. Wang, L. Xiao, and S. Liu, "Fabrication of lotus-like Au@TiO$_2$ nanocomposites with enhanced gas-sensing properties," *Sensors and Actuators B*, vol. 236, pp. 490–498, 2016.

[131] A. I. Ayesh, Z. Karam, F. Awwad, and M. A. Meetani, "Conductometric graphene sensors decorated with nanoclusters for selective detection of Hg^{2+} traces in water," *Sensors and Actuators, B: Chemical*, vol. 221, Article ID 18652, pp. 201–206, 2015.

Journal of
Nanotechnology

International Journal of
Corrosion

International Journal of
Polymer Science

Smart Materials
Research

Journal of
Composites

BioMed
Research International

Journal of
Metallurgy

Journal of
Materials

Journal of
Nanoparticles

Advances in
Materials Science and Engineering

Scientifica

Journal of
Nanomaterials

The Scientific
World Journal

International Journal of
Biomaterials

Journal of
Nanoscience

Journal of
Coatings

Journal of
Crystallography

Journal of
Ceramics

Journal of
Textiles

Hindawi

Submit your manuscripts at
http://www.hindawi.com